

Alignment-dependent ionization of molecules in near-circularly polarized intense laser fields

Jie Liu(刘洁), Yong-Kang Zhang(张永康), and Xiao-Lei Hao(郝小雷)
Citation: Chin. Phys. B, 2025, 34 (**5**): 053201. DOI: 10.1088/1674-1056/adbdc2
http://cpb.iphy.ac.cn; http://iopscience.iop.org/cpb

What follows is a list of articles you may be interested in

Frequency shifts of high-order harmonics from ZnO crystals by chirped laser pulses

Yu Zhao(赵宇), Xiao-Jin Liu(刘晓瑾), Shuang Wang(王爽), Xiao-Xin Huo(霍晓鑫), Yun-He Xing(邢云鹤), and Jun Zhang(张军)
Chin. Phys. B, 2025, 34 (**3**): 033201. DOI: 10.1088/1674-1056/ada9dc

Interference of harmonics emitted by different tunneling momentum channels in laser fields

Ling-Yu Zhang(张玲玉), Zhuo-Xuan Xie(谢卓璇), Can Wang(王灿), Xin-Lei Ge(葛鑫磊), and Jing Guo(郭静)
Chin. Phys. B, 2024, 33 (**9**): 093201. DOI: 10.1088/1674-1056/ad5d95

Generation of elliptical isolated attosecond pulse from oriented H_2^+ in a linearly polarized laser field

Yun-He Xing(邢云鹤), Jun Zhang(张军), Xiao-Xin Huo(霍晓鑫), Qing-Yun Xu(徐清芸), and Xue-Shen Liu(刘学深)
Chin. Phys. B, 2022, 31 (**4**): 043203. DOI: 10.1088/1674-1056/ac398b

Nonadiabatic molecular dynamics simulation of ${{\rm{C}}}_{2}{{\rm{H}}}_{2}^{2+}$ in a strong laser field

Ji-Gen Chen(陈基根), Gang-Tai Zhang(张刚台), Ting-Ting Bai(白婷婷), Jun Wang(王俊), Ping-Ping Chen(陈平平), Wei-Wei Yu(于伟威)§, and Xi Zhao(赵曦)¶
Chin. Phys. B, 2020, 29 (**11**): 113202. DOI: 10.1088/1674-1056/abb3de

Angle-resolved spectra of the direct above-threshold ionization of diatomic molecule in IR+XUV laser fields

Shang Shi(石尚), Fa-Cheng Jin(金发成), Bing-Bing Wang(王兵兵)
Chin. Phys. B, 2019, 28 (**2**): 023202. DOI: 10.1088/1674-1056/28/2/023202

Alignment-dependent ionization of molecules in near-circularly polarized intense laser fields

Jie Liu(刘洁), Yong-Kang Zhang(张永康), and Xiao-Lei Hao(郝小雷)†

Institute of Theoretical Physics, State Key Laboratory of Quantum Optics Technologies and Devices, Shanxi University, Taiyuan 030006, *China*

(Received 23 January 2025; revised manuscript received 27 February 2025; accepted manuscript online 7 March 2025)

The alignment-dependent photoelectron spectrum is a valuable tool for mapping out the electronic structure of molecular orbitals. However, this approach may not be applicable to all molecules, such as CO_2, as the ionization process in a linearly polarized laser field involves contributions from orbitals other than the highest occupied molecular orbital (HOMO). Here, we conducted a theoretical investigation into the ionization process of N_2 and CO_2 in near-circularly polarized laser field using the Coulomb-corrected strong-field approximation (CCSFA) method for molecules. In particular, we introduced a generalized dressed state into the CCSFA method in order to account for the impact of the laser field on the molecular initial state. The simulated alignment-dependent photoelectron momentum distribution (PMD) of the two molecules exhibited markedly disparate behaviors, which were in excellent agreement with the previous experimental observations reported in [*Phys. Rev. A* **102**, 013117 (2020)]. Our findings indicate that under a near-circularly polarized laser field, the alignment-dependent PMD of molecules is primarily sourced from the HOMO, in contrast to the situation under a linearly polarized laser field. Moreover, a satisfactory correlation between the alignment-dependent angular distribution and the orbital symmetry was observed, which suggests an effective approach for molecular orbital imaging.

Keywords: alignment, Coulomb-corrected strong-field approximation (CCSFA), photoelectron momentum distribution (PMD), image

PACS: 32.80.Rm, 33.20.Xx, 33.80.Rv, 33.80.–b

DOI: 10.1088/1674-1056/adbdc2 **CSTR:** 32038.14.CPB.adbdc2

1. Introduction

One of the ultimate goals of molecular physics and chemistry is to follow chemical reactions in molecules by directly imaging the outermost electronic structure. Ultrashort laser pulses have been demonstrated to allow monitoring electronic and nuclear motion with subfemtosecond and subangstrom resolution in real time.[1–7] Specifically, the ability to align molecules[8] enables their ionization and radiation to be measured as a function of molecular alignment relative to the polarization of a linearly polarized intense infrared laser field. These measurements can be utilized to map out the electronic structure of the molecular orbitals involved.[9–11] It has been successfully applied to some molecules, such as N_2 and O_2, but has failed to image the highest occupied molecular orbitals (HOMOs) for other molecules, such as CO_2.[9,12,13] This is due to the direct contribution of the lower-lying orbitals as well as the coupling between them play an important role in the ionization process of CO_2 in linearly polarized laser field.[14–16]

On the other hand, the atttoclock method[5] utilizes a strong, nearly circularly polarized femtosecond laser pulse to map the subcycle emission time of an ionized electron to its emission angle. The attosecond method was initially applied to atoms to solve the fundamental question of how long a tunneling particle remains in the potential region.[5,17–19] It was later extended to molecular systems, in which the orbital symmetry-dependent electronic dynamics introduces additional complexity,[20–22] even for the simplest molecule H_2.[23–26] In particular, when molecules are aligned, their molecular orbitals leave a distinct imprint in the photoelectron momentum distribution. It has been reported experimentally[27] that aligned N_2 exhibits distinct behavior compared to aligned CO_2 in a near-circularly polarized laser field, and the alignment dependence cannot be interpreted by the molecular Ammosov–Delone–Krainov (MO-ADK) theory.[28]

On the theoretical side, the strong-field approximation (SFA) method has been extended to molecular systems to the investigation of the ionization process of molecules.[29,30] The underlying physical mechanisms of the ionization process are inherently distinct in MO-ADK and molecular SFA. The MO-ADK theory treats the ionization of molecules as a tunneling process which is essentially identical to that of atoms. Hence, the ionization is mainly determined by the asymptotic behavior of the bound state wave function at large distances. In contrast, in the SFA theory, the ionization is calculated by the S-matrix theory which treats the external laser field in a nonperturbative way. The interference between ionized wave packets emitted from different nuclei in the molecule, which is not in-

†Corresponding author. E-mail: xlhao@sxu.edu.cn

© 2025 Chinese Physical Society and IOP Publishing Ltd. All rights, including for text and data mining, AI training, and similar technologies, are reserved.

cluded in the MO-ADK theory, plays an essential role in the ionization process in the SFA theory. Nevertheless, the molecular SFA theory also exhibits certain limitations and needs further refinement. Firstly, the Coulomb interaction between the ionized electron and the residual ion, which is not accounted in SFA, has to be incorporated. This has been achieved by extending the Coulomb-corrected SFA (CCSFA) for the ionization of atoms[31] to the case of molecules.[32,33] Secondly, the effect of the laser field on the initial molecular state has to be considered. In the case of molecules with relatively small nuclear separations, such as N_2 and O_2, this effect can be neglected, and the standard molecular SFA, which assumes an unperturbed initial state, has been successfully employed to interpret the various features of molecular ionization.[34–36] However, in the case of molecules with large nuclear separations, it is necessary to consider the impact of the laser on the initial state. This issue is partially addressed by introducing a modification to the initial ground state wave function, which is referred to as the "dressed state".[37–39] In this context, the term "large" refers to a nuclear separation being at least comparable to, or larger than, the range of atomic orbitals. This condition is satisfied in the case of rare gas molecules. However, when the separation between two atoms in a molecule is of medium size, for example, the two oxygen atoms in CO_2, it seems that both the undressed and the fully dressed formulae are unsuitable.

In this paper, by introducing a generalized dressed initial state of molecules in the Coulomb-corrected strong-field approximation (CCSFA) method for molecules, we theoretically investigate the alignment-dependent photoelectron momentum distribution (PMD) for N_2 and CO_2 in a near-circularly polarized laser field. Our simulated results are in good agreement with the experimental results reported in Ref. [27], which validates our extension of the dressed initial state in the CCSFA. In addition, we demonstrate that the observed alignment dependence for N_2 and CO_2 is a direct result of the HOMO, which indicates the effectiveness of imaging molecular orbitals under near-circularly polarized laser fields.

2. Theoretical methods

In the SFA, the transition matrix element in length gauge is given by[40,41]

$$M_p = -\mathrm{i}\int_{-\infty}^{\infty} \mathrm{d}t\, \langle \boldsymbol{p}+\boldsymbol{A}(t)|\, \boldsymbol{r}\cdot\boldsymbol{E}(t)\,|\psi_0(\boldsymbol{r})\rangle \exp[\mathrm{i}S(t)], \quad (1)$$

where

$$S(t) = \int_{-\infty}^{t} \left\{ \frac{1}{2}[\boldsymbol{p}+\boldsymbol{A}(\tau)]^2 + I_\mathrm{p} \right\} \mathrm{d}\tau \quad (2)$$

is the semiclassical action. In the above formulas, $\boldsymbol{E}(t) = -\partial \boldsymbol{A}(t)/\partial t$ represents the laser electric field with the vector potential $\boldsymbol{A}(t) = A_0(\boldsymbol{e}_z \cos\omega t - \varepsilon \boldsymbol{e}_x \sin\omega t)$ and ε the ellipticity of the laser field, $|\psi_0(\boldsymbol{r})\rangle$ is the initial electronic bound state, $|\boldsymbol{p}+\boldsymbol{A}(t)\rangle$ is the Volkov state, and I_p is the ionization potential.

For the laser field with high intensity and low frequency, the temporal integral in Eq. (1) can be evaluated by the saddle-point method,[42,43] thus the solution t_s should satisfy the saddle-point equation

$$\frac{1}{2}[\boldsymbol{p}+\boldsymbol{A}(t_s)]^2 + I_\mathrm{p} = 0. \quad (3)$$

Since $I_\mathrm{p} > 0$, the above equation has complex solutions. Subsequently, the transition amplitude is rewritten as

$$M_{\boldsymbol{p}}^{(0)} = \sum_s \langle \boldsymbol{p}+\boldsymbol{A}(t_s)|\, \boldsymbol{r}\cdot\boldsymbol{E}(t_s)\,|\psi_0(\boldsymbol{r})\rangle \times \sqrt{\frac{2\pi\mathrm{i}}{\partial^2 S/\partial t_s^2}} \exp[\mathrm{i}S(t_s)]. \quad (4)$$

The Coulomb field plays a pivotal role in the emergence of non-zero offset angles in the PMD in elliptically polarized laser fields. Therefore, the Coulomb correction to the SFA is of particular importance. The Coulomb-corrected strong field approximation (CCSFA)[31] incorporates the Coulomb field by correcting the trajectories and actions of ionized electrons

$$M_{\tilde{\boldsymbol{p}}} = \sum_s \langle \boldsymbol{p}+\boldsymbol{A}(t_s)|\, \boldsymbol{r}\cdot\boldsymbol{E}(t_s)\,|\psi_0(\boldsymbol{r})\rangle \times \sqrt{\frac{2\pi\mathrm{i}}{\partial^2 S/\partial t_s^2}} \exp\left[\mathrm{i}S'(t_s)\right], \quad (5)$$

where $\tilde{\boldsymbol{p}}$ is the asymptotic momentum disturbed by the Coulomb field. The modified action, $S'(t_s)$, is given by the following formula:

$$S'(t_s) = -\int_{t_s}^{t_\mathrm{r}} \mathrm{d}\tau \left\{ \frac{1}{2}[\boldsymbol{p}+\boldsymbol{A}(\tau)]^2 - \frac{1}{\sqrt{\boldsymbol{r}^2(\tau)}} \right\} - \int_{t_\mathrm{r}}^{t_\mathrm{F}} \mathrm{d}\tau \left[\frac{\tilde{\boldsymbol{v}}^2(\tau)}{2} + V(\boldsymbol{r}) \right] + I_\mathrm{p}(t_s - t_\mathrm{F}), \quad (6)$$

where t_s is the complex saddle point solution, t_r is its real part, and t_F is the end of the laser pulse. The first integral in the right-hand of Eq. (6) represents the sub-barrier action, while the second integral represents the action obtained after the electron has left the tunnel exit. In this model, after tunneling, the motion of the electron in the laser and Coulomb fields is governed by Newton's equations, specifically $\mathrm{d}\tilde{\boldsymbol{v}}(t)/\mathrm{d}t = \boldsymbol{E}(t) - \partial V(\boldsymbol{r})/\partial \boldsymbol{r}$, where $\tilde{\boldsymbol{v}}(t)$ is the instantaneous velocity and $V(r) = -1/r$. The electrons propagate in the laser field until the end of the pulse at time t_F. Subsequently, the final asymptotic momentum $\tilde{\boldsymbol{p}}$ of the electrons is obtained analytically by utilizing Kepler's law. Finally, these trajectories are coherently summed to obtain different types of distributions.

In the molecular CCSFA,[32,33] the initial state $|\psi_0(\boldsymbol{r})\rangle$ in Eq. (5) is represented by the wave function of the specific

molecular orbital, while the trajectories and the semiclassical action in Eq. (5) are the same as those in the case of atoms. The initial molecular electronic wave function can be expressed as a linear combination of atomic orbitals (LCAO) within the fixed-nucleus approximation.[44] For N_2, the initial molecular electronic state is written as

$$\psi_0(\boldsymbol{r}) = \sum_a c_a \left[\psi_a^{(0)}\left(\boldsymbol{r}+\frac{\boldsymbol{R}_a}{2}\right)+\gamma\psi_a^{(0)}\left(\boldsymbol{r}-\frac{\boldsymbol{R}_a}{2}\right)\right], \quad (7)$$

where $\boldsymbol{R}_a$ denotes the relative nuclear coordinate, the subscript a denotes different orbitals of the nitrogen atom pair, γ can be 1 or -1 depending on the symmetry. And for CO_2, the wave function can be written as

$$\begin{aligned}\psi_0(\boldsymbol{r}) = &\sum_a c_a \left[\psi_a^{(0)}\left(\boldsymbol{r}+\frac{\boldsymbol{R}_a}{2}\right)+\gamma\psi_a^{(0)}\left(\boldsymbol{r}-\frac{\boldsymbol{R}_a}{2}\right)\right] \\ &+\sum_b c_b \psi_b^{(0)}(\boldsymbol{r}),\end{aligned} \quad (8)$$

where $\boldsymbol{R}_a$ denotes the relative nuclear coordinate between the two oxygen atoms, the subscript a denotes different orbitals of the oxygen atom pair, and b denotes the different orbitals of the carbon atom.

Previous research on molecular ionization[37–39] has demonstrated the necessity of considering the impact of the laser on the initial state within the framework of the SFA approach for molecules with large nuclear separations, for example, rare gas molecules with a separation of more than 6 a.u. The initial ground state wave function was modified by the introduction of a dressing factor $\exp[-\mathrm{i}\boldsymbol{A}(t)\cdot(\pm\frac{\boldsymbol{R}_a}{2})]$ in front of the atomic orbital. For molecules with small separations, such as N_2, however, the dressed state is not applicable and therefore the undressed state should be employed instead. For CO_2, the separation of the two oxygen (O) atoms is medium, so neither the undressed nor the fully dressed formula can be employed. In order to accommodate molecules with intermediate nuclear separations, we generalize the dressed initial state by incorporating an additional parameter, designated as α, which is constrained within the range of 0 to 1, into the dressing factor $\exp[-\mathrm{i}\alpha\boldsymbol{A}(t)\cdot(\pm\frac{\boldsymbol{R}_a}{2})]$. The resulting generalized dressed initial state for N_2 and CO_2 can be written respectively as

$$\begin{aligned}\psi_0(\boldsymbol{r}) = &\sum_a c_a \left[\exp\left[-\mathrm{i}\alpha\boldsymbol{A}(t)\cdot\left(+\frac{\boldsymbol{R}_a}{2}\right)\right]\psi_a^{(0)}\left(\boldsymbol{r}+\frac{\boldsymbol{R}_a}{2}\right)\right. \\ &\left.+\gamma\exp\left[-\mathrm{i}\alpha\boldsymbol{A}(t)\cdot\left(-\frac{\boldsymbol{R}_a}{2}\right)\right]\psi_a^{(0)}\left(\boldsymbol{r}-\frac{\boldsymbol{R}_a}{2}\right)\right],\end{aligned} \quad (9)$$

$$\begin{aligned}\psi_0(\boldsymbol{r}) = &\sum_a c_a \left[\exp[-\mathrm{i}\alpha\boldsymbol{A}(t)\cdot\left(+\frac{\boldsymbol{R}_a}{2}\right)\right]\psi_a^{(0)}\left(\boldsymbol{r}+\frac{\boldsymbol{R}_a}{2}\right) \\ &+\gamma\exp\left[-\mathrm{i}\alpha\boldsymbol{A}(t)\cdot\left(-\frac{\boldsymbol{R}_a}{2}\right)\right]\psi_a^{(0)}\left(\boldsymbol{r}-\frac{\boldsymbol{R}_a}{2}\right)\Big] \\ &+\sum_b c_b \psi_b^{(0)}(\boldsymbol{r}).\end{aligned} \quad (10)$$

The transition matrix element of Eq. (5) for N_2 and CO_2 can be rewritten correspondingly as

$$\begin{aligned}M_{\tilde{\boldsymbol{p}}} = &\sum_s\sum_a f_{\gamma,a}(\boldsymbol{p},\boldsymbol{R}_a)\langle\boldsymbol{p}+\boldsymbol{A}(t_s)|\,\boldsymbol{r}\cdot\boldsymbol{E}(t_s)\,|\psi_a\rangle \\ &\times\sqrt{\frac{2\pi\mathrm{i}}{\partial^2 S/\partial t_s^2}}\exp\left[\mathrm{i}S'(t_s)\right],\end{aligned} \quad (11)$$

$$\begin{aligned}M_{\tilde{\boldsymbol{p}}} = &\sum_s\left(\sum_a f_{\gamma,a}(\boldsymbol{p},\boldsymbol{R}_a)\langle\boldsymbol{p}+\boldsymbol{A}(t_s)|\,\boldsymbol{r}\cdot\boldsymbol{E}(t_s)\,|\psi_a\rangle\right. \\ &\left.+\sum_b\langle\boldsymbol{p}+\boldsymbol{A}(t_s)|\,\boldsymbol{r}\cdot\boldsymbol{E}(t_s)\,|\psi_b\rangle\right) \\ &\times\sqrt{\frac{2\pi\mathrm{i}}{\partial^2 S/\partial t_s^2}}\exp\left[\mathrm{i}S'(t_s)\right],\end{aligned} \quad (12)$$

where

$$\begin{aligned}&f_{\gamma,a}(\boldsymbol{p},\boldsymbol{R}_a) \\ &=\begin{cases}2\mathrm{i}\sin\left[(\boldsymbol{p}+(1-\alpha)\boldsymbol{A}(t_s))\cdot\dfrac{\boldsymbol{R}_a}{2}\right], & \gamma=-1,\\ 2\cos\left[(\boldsymbol{p}+(1-\alpha)\boldsymbol{A}(t_s))\cdot\dfrac{\boldsymbol{R}_a}{2}\right], & \gamma=1\end{cases}\end{aligned} \quad (13)$$

is the interference term, which plays a significant role in the process of molecular ionization but is not included in the MO-ADK theory. In the case of molecules with a small nuclear separation, such as N_2, α should be equal to 0, which reduces the model to the undressed case. While for molecules with a large nuclear separation, α should be equal to 1, which represents the fully dressed state. For molecules with a medium nuclear separation, such as CO_2, α takes a value between 0 and 1, which represents a partially dressed state.

In our calculations for N_2 and CO_2, in addition to HOMO, the lower-lying orbitals HOMO-1, HOMO-2, and HOMO-3 are also taken into account. The wave functions of these orbitals are obtained numerically by the GAMESS code.[45] The nuclear separation of N_2 in the calculation is 2.075 a.u., and the nuclear separation of two oxygen atoms in CO_2 is 4.39 a.u. The spatial distributions of these orbitals are presented in Fig. 1. The laser filed is polarized in the x–z plane, with z axis the major axis and x axis the minor axis of the elliptically polarized laser field. The profile of the laser pulse is taken as

$$F(t)=\begin{cases}1, & t\le 4T,\\ \cos^2\dfrac{(t-4T)\pi}{4T}, & 4T<t\le 6T,\\ 0, & t>6T,\end{cases} \quad (14)$$

where T is the optical period. The flat top and the falling edge of the pulse were both extended for the purpose of verification, and it was found that this did not result in a notable alteration to the results.

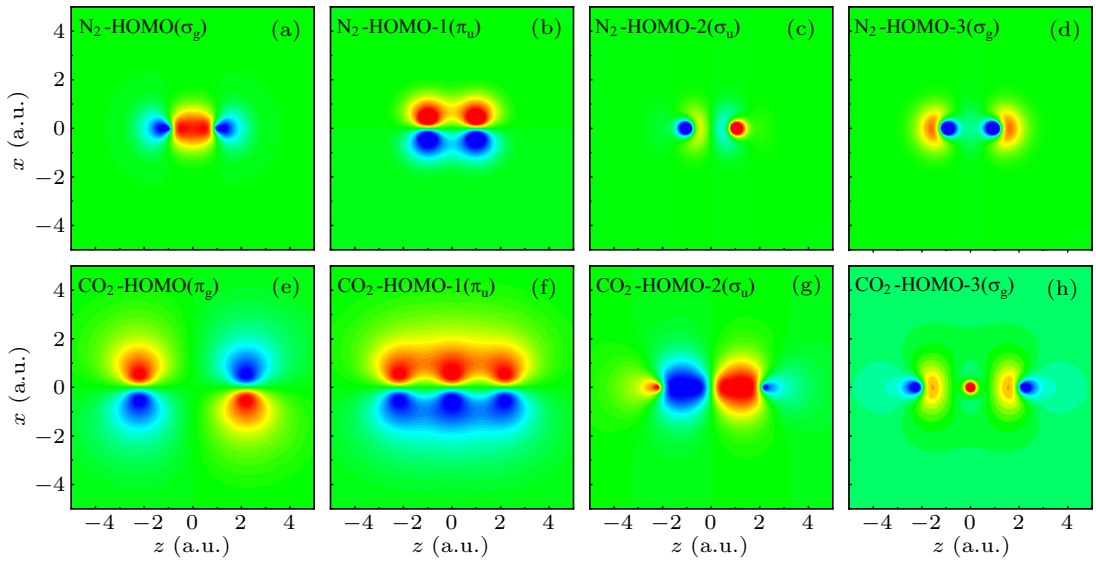


Fig. 1. Spatial distributions of the electronic wave functions calculated by the GAMESS code for different orbitals of N_2 and CO_2.

3. Results and discussion

Figure 2 illustrates the PMDs of N_2 and CO_2 at various alignment angles. The laser wavelength is 800 nm, with a peak laser intensity of 1.8×10^{14} W/cm^2 and an ellipticity of 0.82 for N_2 and a peak laser intensity of 1.6×10^{14} W/cm^2 and an ellipticity of 0.85 for CO_2, the same laser parameters employed in Ref. [27]. The dressing parameter is set to 0 and 0.5 for N_2 and CO_2, respectively. The inset in the upper left corner of each panel depicts the molecular alignment. The alignment angle is defined as the angle between the molecular axis and the major axis of the laser field. The first and second rows of Fig. 2 illustrate the PMDs of N_2 and CO_2, respectively, with alignment angles ranging from 0° to 150° in 30° intervals. It is evident that the PMD is significantly influenced by the the alignment angle, demonstrating the profound impact of the molecular orbital on the PMD. For atoms, the PMD is primarily determined by the laser electric field. If the effect of the Coulomb potential is not considered, ionized electrons accelerated by the laser field drift perpendicular to the instantaneous field at the time of release. The photoelectrons subsequently disperse along the minor axis. Upon consideration of the Coulomb potential, electrons undergo a deflection, which induces a deflection of the photoelectron from the minor axis of the laser field. The resulting PMD of atoms is analogous to that observed for N_2 aligned along the minor axis, as illustrated in Fig. 2(a), which exhibits a counterclockwise deviation with respect to the minor axis. In addition to the influences of the laser field and Coulomb potential, the characteristics of the molecular orbital also play a pivotal role, as elucidated by Eqs. (11) and (12). Consequently, as the alignment angle increases, the PMDs for molecules may change in a manner distinct from atoms. For instance, at an alignment angle of 120°, the PMD for N_2 in Fig. 2(e) undergoes a clockwise deviation, which is in opposition to the effect of the Coulomb potential. This tendency is in agreement with the measured results presented in Ref. [27], wherein PMDs of of N_2 with alignment angles of 45° and 135° are shown. The experimental results exhibit two maxima near the p_x axis at both alignment angles, yet these maxima differ in terms of the deflection angles. The PMD at an alignment angle of 135° exhibits a clockwise deviation compared with that observed at 45°. In addition, the PMDs for the two molecules at the same alignment angle exhibit significant differences due to their distinct molecular orbitals. The range of emission angles in the PMD of CO_2 at most alignment angles is wider than that observed for N_2. This disparity further demonstrates the close relation between the PMD and the molecular electronic structure.

In order to elucidate the impact of the molecular orbital on the PMD and to verify the validity of the generalized dressed state, we present the photoelectron angular distribution (PAD) as a function of the alignment angle after integrating the photoelectron momentum. This is illustrated in Fig. 3. For N_2, only the undressed case ($\alpha = 0$) is presented in Fig. 3(a), the validity of which has been demonstrated by prior research.[37] The cases of undressed ($\alpha = 0$), partially dressed ($\alpha = 0.5$), and fully dressed ($\alpha = 1$) for CO_2 are presented in Figs. 3(b), 3(c), and 3(d), respectively. Both molecules display periodic changes with 180°, consistent with their non-polar nature. Figure 3(a) illustrates that the alignment-dependent PAD for N_2 exhibits a single-hump structure within the alignment angle range (90°, 270°), with the maximum yield occurring at alignment angles of 0° and 180°. The distribution pattern for CO_2 depends on the dressing parameter α. In the undressed case with $\alpha = 0$ (Fig. 3(b)), the alignment-dependent PAD is analogous to that observed for N_2 but exhibits a broader profile, displaying a single-hump structure. In the case of the partially dressed state with $\alpha = 0.5$ (Fig. 3(c)), the photoelectron yield

of CO_2 reaches its maximum near alignment angles of 30°, 150°, 210°, and 330°, exhibiting a double-hump structure. The PAD for the fully dressed state with $\alpha = 1$ in Fig. 3(d) also exhibits a double-hump structure, but the positions are different. The photoelectron yield reaches its maximum near alignment angles of 45°, 120°, 225°, and 300°. In the comparison to the preceding experimental findings (see Fig. 2 in Ref. [27]), it can be concluded that the alignment-dependent PADs for undressed N_2 and partially dressed CO_2 are in accordance with the experimental observations, thereby supporting the validity of the generalized dressed initial molecular state. In addition, in order to ascertain whether this conclusion is contingent on the laser intensity, calculations were also made at lower laser intensities, as demonstrated in Figs. 3(e)–3(h). It is evident that for both N_2 and CO_2, the structures observed within the alignment-dependent PADs are independent of laser intensity. In the following section, the undressed N_2 and partially dressed CO_2 will be employed in the analysis.

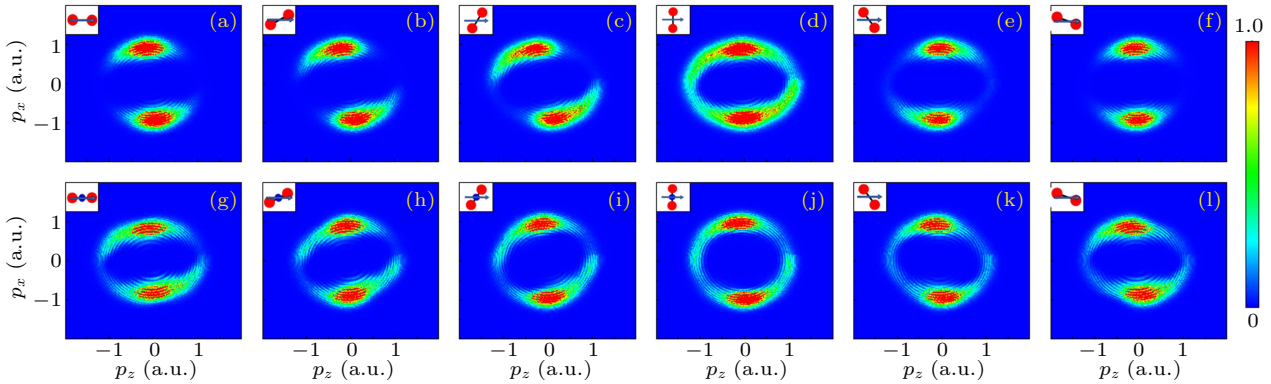


Fig. 2. Photoelectron momentum distributions of N_2 (a)–(f) and CO_2 (g)–(l) at alignment angles from 0° to 150° with an interval of 30°. The alignment angle is defined as the angle between the molecular axis and the main axis of the laser field, as indicated by the inset in each panel. The same laser parameters as those utilized in Ref. [27] are employed. In particular, the center wavelength of the laser field is 800 nm. For N_2, the peak laser intensity is 1.8×10^{14} W/cm^2, and the ellipticity is 0.82. For CO_2, the peak laser intensity is 1.6×10^{14} W/cm^2, and the ellipticity is 0.85.

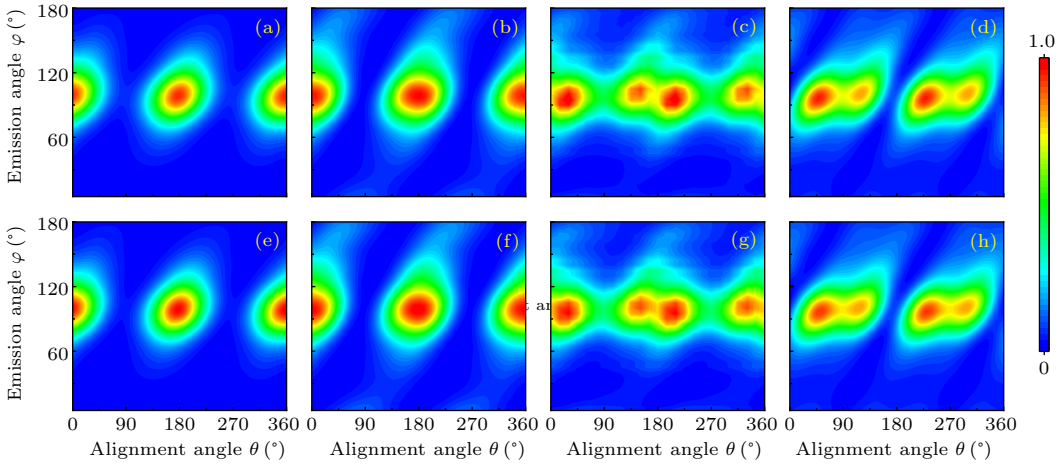


Fig. 3. Photoelectron angular distribution (PAD) of momentum-integrated yield as a function of the alignment angle with various laser intensities for undressed ($\alpha = 0$) N_2 in panels (a), (e), and for CO_2 in different cases: undressed ($\alpha = 0$), partially dressed ($\alpha = 0.5$), and fully dressed ($\alpha = 1$) in panels (b) and (f), (c) and (g), (d) and (h), respectively. The first row exhibits the laser intensity of 1.8×10^{14} W/cm^2 for N_2 (a) and 1.6×10^{14} W/cm^2 for CO_2 (b), (c), and (d). The second row exhibits the relatively low laser intensity of 1.6×10^{14} W/cm^2 for N_2 (e) and 1.4×10^{14} W/cm^2 for CO_2 (f), (g), and (h). The ellipticity is 0.82 for N_2 and 0.85 for CO_2, and the wavelength is 800 nm.

In Fig. 4, the contributions of the different orbitals of the two molecules are separated in order to identify their specific roles in the ionization process. Figures 4(a) and 4(f) illustrate the integrated yields corresponding to the HOMO, the HOMO-1, the HOMO-2, and the HOMO-3 of N_2 and CO_2, respectively, as a function of the alignment angle. It is evident that the contribution of the HOMO is significantly higher than that of the other three low-lying orbitals at all alignment angles for both molecules. In the case of CO_2 in particular, the contribution of the HOMO is two orders of magnitude higher than that of the low-lying orbitals. The alignment-dependent PADs corresponding to different orbitals are presented in Figs. 4(b)–4(e) for N_2, and in Figs. 4(g)–4(j) for CO_2. It is evident that the pattern of distribution depends significantly on the molecular orbitals. As anticipated, the distributions of the HOMOs, a σ_g orbital for N_2 and a π_g orbital for CO_2, as shown in Figs. 4(b) and 4(g), are nearly identical to the total distributions in Figs. 3(a) and 3(b), respectively. This provides further evidence that the experimentally observed distribution is solely attributable to the HOMO for both molecules. The π_u

orbital of HOMO-1 (Fig. 4(c)) for N_2, despite its single-hump structure, exhibits a markedly broader distribution than that of the HOMO. The PAD for HOMO-2 (Fig. 4(d)), which is a σ_u orbital, exhibits a slight broadening of the distribution in comparison to that of the HOMO. The distribution for HOMO-3 (Fig. 4(e)), a σ_g orbital, is identical to that of the HOMO, which is also a σ_g orbital. In the case of CO_2, the distribution of the HOMO-1 (Fig. 4(h)), a π_u orbital, exhibits a double-hump structure similar to that of the HOMO, with only minor differences in detail. The distributions of the HOMO-2 (σ_u) and HOMO-3 (σ_g), as shown in Figs. 4(i) and 4(j), respectively, are characterized by a single-hump structure, which are similar to the distribution of the HOMO of N_2. Therefore, there is a strong correlation between the orbital features, including the nuclear separation and the symmetry, and the alignment-dependent PAD.

It is noteworthy that the contribution of molecular ionization may not primarily originate from the HOMO in linearly polarized laser fields, at least in the case of CO_2. Figure 5 illustrates the contributions of various orbitals for the two molecules at different ellipticities of the laser field. In the case of N_2, the contribution of the HOMO is predominant at all alignment angles across different laser ellipticities. In the case of CO_2, however, the situation is different for ellipticity of 0.3 and linearly polarized laser fields. In these cases, the ionization yield of HOMO-2 is nearly equal to that of the HOMO at parallel alignment angles where the laser electric field is directed towards the nodes of the HOMO. This will result in the alignment-dependent PAD becoming a combined contribution of different orbitals. In the case of near-circularly polarized laser field, however, a considerable laser field is present in all directions at any alignment angles. Consequently, the ionization potential exerts a more decisive influence on the contributions of different orbitals. Therefore, the HOMO is superior in near-circularly polarized laser fields. This implies that the alignment-dependent PAD in a near-circularly polarized laser field is an ideal tool for imaging molecular HOMO.

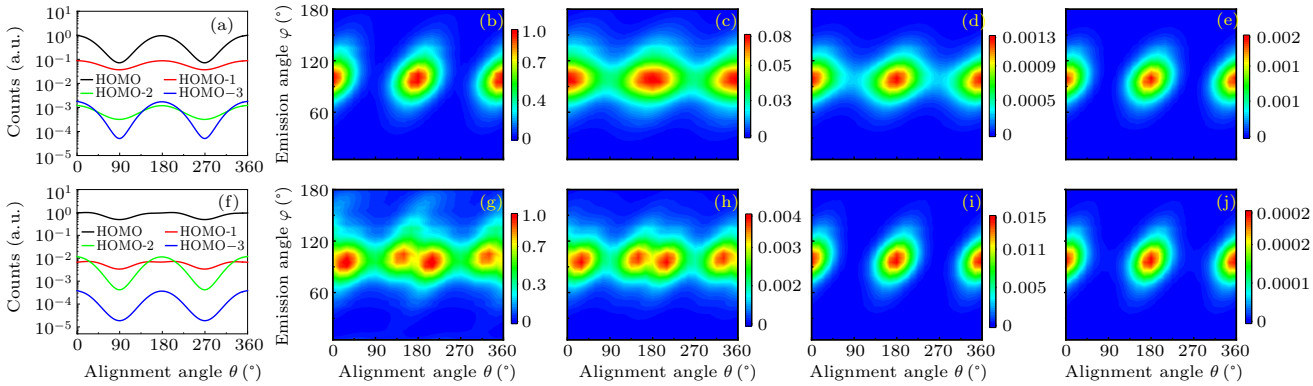


Fig. 4. Contributions of different orbitals for N_2 and CO_2 as a function of the alignment angle. (a) Integrated ionization yields for different orbitals of N_2. (b)–(e) PAD of momentum-integrated yield for HOMO, HOMO-1, HOMO-2, and HOMO-3 of N_2, respectively. (f) Integrated ionization yield for different orbitals of CO_2. (g)–(j) PAD for HOMO, HOMO-1, HOMO-2, and HOMO-3 of CO_2, respectively. The laser parameters are the same as those illustrated in Fig. 2.

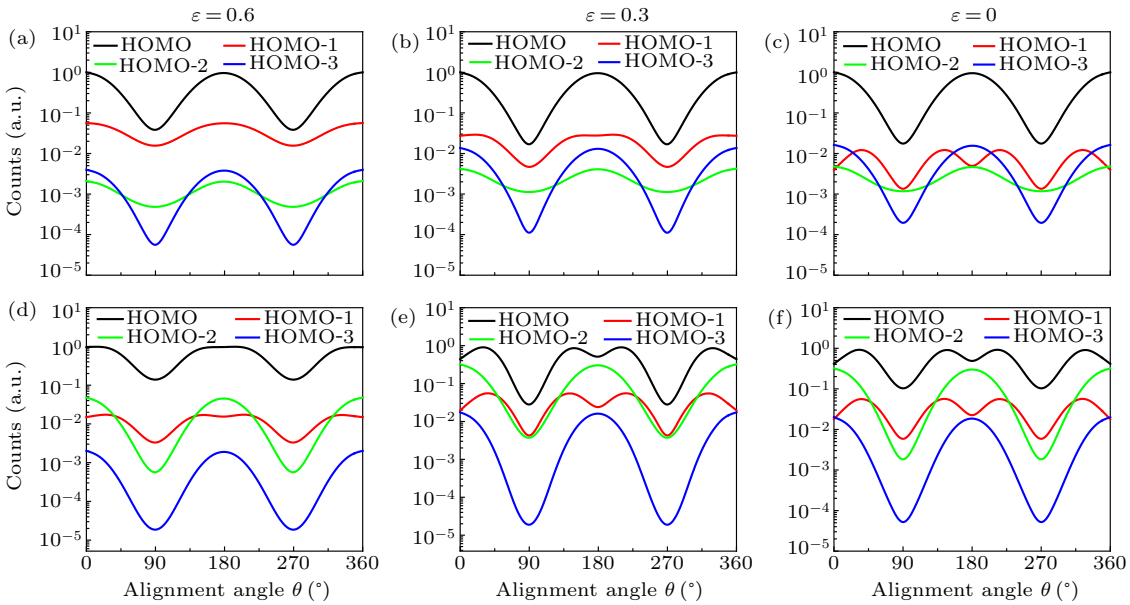


Fig. 5. Integrated ionization yield for the different orbitals of N_2 (the first row) and CO_2 (the second row) at different ellipticities ε of the laser field. The laser wavelength and intensities employed are the same as those illustrated in Fig. 2.

In the context of actual experiments, the effect of the focal averaging of the laser intensity has to be considered. The alignment-dependent PADs for the two molecules after considering the focal averaging effect are presented in Figs. 6(a) and 6(b), respectively. It is evident that the focal averaging has minor effect on the pattern of the PAD, which is attributable to the fact that the PAD is insensitive to the laser intensity. In addition, all the results presented above are obtained by assuming that the molecules are perfectly aligned. However, in the actual experiments, the molecules are aligned imperfectly, and the distribution of their orientations must be considered. Here the well-established $\cos^4\theta$ distribution[46,47] is employed to mimic the molecular orientation distribution. The corresponding results are presented in Figs. 6(c) and 6(d) for the two molecules respectively. In the case of the N_2 molecule, the alignment-dependent PAD still exhibits a single-hump structure, although it becomes broader in comparison with the case of perfect alignment in Fig. 3(a). As for CO_2 molecule, the alterations resulting from the incorporation of the molecular orientation distribution are particularly notable. The originally discernible double-hump structure becomes blurred and almost indistinguishable. This indicates that a high degree of alignment is necessary to achieve the imaging of molecular HOMO using a near-circularly polarized laser field.

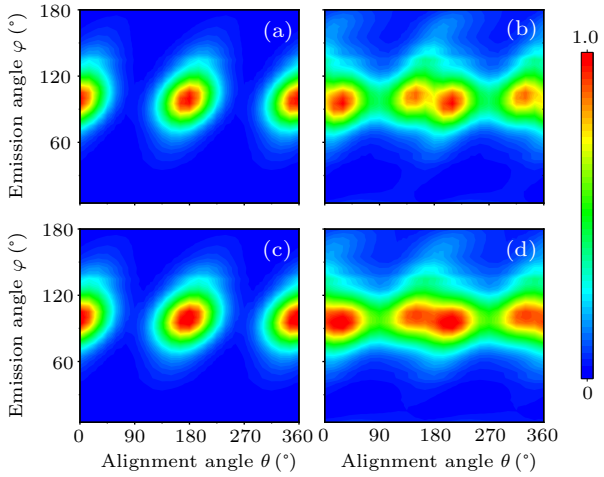


Fig. 6. PAD for momentum-integrated yield obtained after considering the focal averaging effect (the first row) or the $\cos^4\theta$ distribution of molecular orientations (the second row). Panels (a) and (c) are for N_2, panels (b) and (d) are for CO_2. The laser parameters are the same as those illustrated in Fig. 2.

4. Conclusions

In conclusion, we introduced a generalized dressed initial state of molecules in the CCSFA method for the investigation of the ionization process of aligned N_2 and CO_2 molecules in a near-circularly polarized laser field. The simulated alignment-dependent PADs for undressed N_2 and partially dressed CO_2 are found to be in good agreement with the experimental observations reported in Ref. [27]. This provides evidence to support the validity of the proposed generalized dressed initial molecular state. It is important to note that the generalized dressed-state molecular CCSFA can be applied not only to non-polar molecules with arbitrary nuclear separations, but also to polar molecules, provided that the laser parameters used ensure that the tunneling picture remains valid. Significant differences were observed in the the behavior of N_2 and CO_2 molecules. The alignment-dependent PAD of N_2 exhibits a single-hump structure, whereas that of CO_2 exhibits a double-hump structure. Our findings indicate that under a near-circularly polarized laser field, the alignment-dependent PAD of molecules is primarily sourced from the HOMO, which is quite different from the situation under a linearly polarized laser field. Furthermore, a good correspondence between the alignment-dependent angular distribution and the orbital features is observed, which indicates an excellent scheme for molecular orbital imaging.

Acknowledgement

Project supported by the National Natural Science Foundation of China (Grant No. 12274273).

References

[1] Rost J M and Saalmann U 2019 *Nat. Photon.* **13** 439
[2] Blaga C I, Xu Junliang, DiChiara A D, Sistrunk E, Zhang K, Agostini P, Miller T A, DiMauro L F and Lin C D 2012 *Nature* **483** 194
[3] Niikura H, Légaré F, Hasbani R, Bandrauk A D, Ivanov M Y, Villeneuve D M and Corkum P B 2002 *Nature* **417** 917
[4] Niikura H, Légaré F, Hasbani R, Ivanov M Y, Villeneuve D M and Corkum P B 2003 *Nature* **421** 826
[5] Eckle P, Smolarski M, Schlup P, Biegert J, Staudte A, Schöffler M, Muller H G, Dörner R and Keller U 2008 *Nat. Phys.* **4** 565
[6] Zhou S S, Lan W D, Chen J G, Wang J, Guo F M and Yang Y J 2022 *Phys. Rev. A* **106** 023510
[7] Uiberacker M, Uphues Th, Schultze M Verhoef A J, Yakovlev V, Kling M F, Rauschenberger J, Kabachnik N M, Schröder H, Lezius M, Kompa K L, Muller H G, Vrakking M J J, Hendel S, Kleineberg U, Heinzmann U, Drescher M and Krausz F 2007 *Nature* **446** 627
[8] Pruna F R and Vrakking M J J 2001 *Phys. Rev. Lett.* **87** 153902
[9] Pavičić D, Lee K F, Rayner D M, Corkum P B and Villeneuve D M 2007 *Phys. Rev. Lett.* **98** 243001
[10] Meckel M, Comtois D, Zeidler D, Staudte A, Pavičić D, Bandulet H C, Pépin H, Kieffer J C, Dörner R, Villeneuve D M and Corkum P B 2008 *Science* **320** 1478
[11] Akagi H, Otobe T, Staudte A, Shiner A, Turner F, Dörner R, Villeneuve D M and Corkum P B 2009 *Science* **325** 1364
[12] Itatani J, Levesque J, Zeidler D, Niikura H, Pépin H, Kieffer J C, Corkum P B and Villeneuve D M 2004 *Nature* **432** 867
[13] Thomann I, Lock R, Sharma V, Gagnon E, Pratt S T, Kapteyn H C, Murnane M M and Li Wen 2008 *J. Phys. Chem. A* **112** 9382
[14] Son S K and Chu S I 2009 *Phys. Rev. A* **80** 011403
[15] Petretti S, Vanne Y V, Saenz A, Castro A and Decleva P 2010 *Phys. Rev. Lett.* **104** 223001
[16] Majety V P and Scrinzi A 2015 *Phys. Rev. Lett.* **115** 103002
[17] Pfeiffer A N, Cirelli C, Smolarski M, Dimitrovski D, Abu-samha M, Madsen L B and Keller U 2012 *Nat. Phys.* **8** 76
[18] Shafir D, Soifer H, Bruner B D, Dagan M, Mairesse Y, Patchkovskii S, Ivanov M Yu, Smirnova O and Dudovich N 2012 *Nature* **485** 343
[19] Yu M, Liu K, Li M, Yan J Q, Cao C P, Tan J, Liang J T, Guo K Y, Cao W, Lan P F, Zhang Q B, Zhou Y M and Lu P X 2022 *Light Sci. Appl.* **11** 215
[20] Zhou H S, Li Q Y, Guo F, Wang J, Chen J G and Yang Y J 2021 *Chem. Phys.* **545** 111147
[21] Fu T T, Zhou S S, Chen J G, Wang J, Guo F M and Yang Y J 2023 *Opt. Express* **31** 30171

[22] Chen J Q, Jiang W L, Qiao Y, Yang Y J and Chen J G 2025 *Chin. Phys. Lett.* **42** 013201

[23] Wu J, Magrakvelidze M, Schmidt L P H, Kunitski M, Pfeifer T, Schöffler M, Pitzer M, Richter M, Voss S, Sann H, Kim H, Lower J, Jahnke T, Czasch A, Thumm U and Dörner R 2013 *Nat. Commun.* **4** 2177

[24] Serov V V, Bray A W and Kheifets A S 2019 *Phys. Rev. A* **99** 063428

[25] Quan W, Serov V V, Wei M Z, Zhao M, Zhou Y, Wang Y L, Lai X Y, Kheifets A S and Liu X J 2019 *Phys. Rev. Lett.* **123** 223204

[26] Khan A, Trabert D, Eckart S, Kunitski M, Jahnke T and Dörner R 2020 *Phys. Rev. A* **101** 023409

[27] Yan J Q, Xie W H, Li M, Liu K, Luo S Q, Cao C P, Guo K Y, Cao W, Lan P F, Zhang Q B, Zhou Y M and Lu P X 2020 *Phys. Rev. A* **102** 013117

[28] Tong X M, Zhao Z X and Lin C D 2002 *Phys. Rev. A* **66** 033402

[29] Muth-Böhm J, Becker A and Faisal F H M 2000 *Phys. Rev. Lett.* **85** 2280

[30] Kjeldsen T K and Madsen L B 2004 *J. Phys. B: At. Mol. Opt. Phys.* **37** 2033

[31] Yan T M, Popruzhenko S V, Vrakking M J J and Bauer D 2010 *Phys. Rev. Lett.* **105** 253002

[32] Wang C, Okunishi M, Hao X, Ito Y, Chen J, Yang Y, Lucchese R R, Zhang M, Yan B, Li W D, Ding D and Ueda K 2016 *Phys. Rev. A* **93** 043422

[33] Yang Y Z, Ren H, Zhang M, Zhou S P, Mu X X, Li X K, Wang Z Z, Deng K, Li M X, Ma P, Li Z, Hao X L, Li W D, Chen J, Wang C C and Ding D J 2023 *Nat. Commun.* **14** 4951

[34] DeWitt M J, Wells E and Jones R R 2001 *Phys. Rev. Lett.* **87** 153001

[35] Lin Z Y, Jia X Y, Wang C L, Hu Z L, Kang H P, Quan W, Lai X Y, Liu X J, Chen J, Zeng B, Chu W, Yao J P, Cheng Y and Xu Z Z 2012 *Phys. Rev. Lett.* **108** 223001

[36] Wei M Z, Wei Q, Sun R P, Xu S P, Xiao Z L, Zhou Y, Zhao M, Hao X Lei, Duan C X and Liu X J 2018 *Phys. Rev. A* **98** 063418

[37] Milošević D B 2006 *Phys. Rev. A* **74** 063404

[38] Chirilă C C and Lein M 2006 *Phys. Rev. A* **73** 023410

[39] Becker W, Chen J, Chen S G and Milošević D B 2007 *Phys. Rev. A* **76** 033403

[40] Busuladžić M, Gazibegovic-Busuladžić A, Milošević D B and Becker W 2008 *Phys. Rev. A* **78** 033412

[41] Busuladžić M and Milošević D B 2010 *Phys. Rev. A* **82** 015401

[42] Lewenstein M, Kulander K C, Schafer K J and Bucksbaum P H 1995 *Phys. Rev. A* **51** 1495

[43] Figueira de Morisson Faria C, Schomerus H and Becker W 2002 *Phys. Rev. A* **66** 043413

[44] Usachenko V I and Chu S I 2005 *Phys. Rev. A* **71** 063410

[45] Schmidt M W, Baldridge K K, Boatz J A, Elbert S T, Gordon M S, Jensen J H, Koseki S, Matsunaga N, Nguyen K A, Su S, Windus T L, Dupuis M and Montgomery J A 1993 *J. Comput. Chem.* **14** 1347

[46] Smirnova O, Mairesse Y, Patchkovskii S, Dudovich N, Villeneuve D, Corkum P and Ivanov M Y 2009 *Nature* **460** 972

[47] Jin C, Le A T and Lin C D 2011 *Phys. Rev. A* **83** 053409